Reduction of Copper in Porous Matrixes. Stepwise and Autocatalytic Reduction Routes

O. P. Tkachenko,[†,‡] K. V. Klementiev,[†,§] M. W. E. van den Berg,[†] N. Koc,[†,||] M. Bandyopadhyay,[⊥] A. Birkner,[#] C. Wöll,[#] H. Gies,[⊥] and W. Grünert*[,†]

Lehrstuhl für Technische Chemie, Lehrstuhl für Kristallographie, and Lehrstuhl für Physikalischen Chemie I, Ruhr-Universität Bochum, D-44780 Bochum, Germany, and HASYLAB, D-22607 Hamburg, Germany

Received: July 21, 2005; In Final Form: September 14, 2005

The reduction of Cu(II) oxide species in siliceous matrixes of different porosity (MFI, FAU, MCM-48) and in alumosilicate MFI was studied by temperature-programmed reduction in hydrogen (TPR), by X-ray absorption fine structure (after stationary hydrogen treatments), and by transmission electron microscopy. It was found that the reduction may proceed in one or in two reduction steps. The two-step scheme known for zeolites was observed also for Cu(II) in siliceous microporous matrixes, with similar temperature of Cu(II) reduction onset as for the alumosilicate MFI. Therefore, the two-step scheme cannot be explained by the stabilization of Cu ions by intra-zeolite electrical fields. CuOx clusters in MCM-48 were reduced in a one-step scheme (similar to bulk CuO) at high Cu content (6 wt %) but in a two-step scheme at low Cu content (1 wt %). The two reduction steps observed with most samples cannot be identified with the transitions of *all* Cu(II) to Cu(I) and of Cu(I) to Cu(0). Instead, Cu(0) nuclei were observed already at low reduction temperatures and were found to coexist with Cu ions over temperature ranges of different extension. This coexistence range was narrow in materials that favor aggregation of the Cu nuclei into particles: Cu-MCM-48 of low Cu content and Cu-ZSM-5. In the latter, metal segregation from the pore system was found to be accompanied by an autocatalytic initiation of the *second* reduction step. In the siliceous microporous matrixes, the Cu(0) nuclei were observed to coexist with Cu ions over wide temperature ranges (100 K for MFI) at temperatures far above that of Cu reduction in the bulk oxide. These observations suggest that oligomeric Cu metal nuclei which may have been formed, e.g., at the intersections of the MFI channel system, may be unable to activate hydrogen, which would be required for rapid reduction of the coexisting Cu ions.

Introduction

Zeolites are known to stabilize transition metals in cationic states, which opens reaction routes not easily observed in the analogous bulk phases. Thus, Rh(I), Pd(I), and Ni(I) cations were observed in the matrix of X zeolite.[1−4] Metallic Cu clusters in ZSM-5 zeolite may be oxidized by zeolite protons when CO is offered in the gas phase, obviously due to the stabilization of Cu(I)−CO complexes by the charged framework.[5] The well-known two-step reduction sequence of Cu(II) ions in zeolites, which was observed in various temperature-programmed reduction (TPR) studies[6−10] and confirmed by in situ X-ray absorption fine structure (XAFS) work[9−11] differs strongly from the reduction of bulk CuO where intermediate Cu(I) can be traced only in time-resolved studies[12,13] or under very short supply of H_2.[14,15] The two steps of the sequence have often been interpreted as a reduction of all Cu(II) to Cu(I), which is stabilized by the intrinsic electrical field of the zeolite, and subsequently to Cu(0).

If the electrical field is crucial for the stabilization of Cu(I), intermediate Cu(I) should not occur in the reduction of Cu(II) species in siliceous matrixes. In an attempt to verify this hypothesis, we studied the reduction of Cu(II) in purely siliceous microporous and mesoporous matrixes (MFI, FAU, MCM-48) and compared this with the reduction behavior in a zeolite (Cu-ZSM-5; data on Cu-Y, which are strongly affected by special effects of the remote sites in FAU will be reported elsewhere[16]). It was found by TPR that the stepwise reduction scheme is not particular to alumosilicate zeolites while extended X-ray absorption fine structure (EXAFS) studies revealed that Cu(0) is present already after the first reduction step. The data obtained suggest that hydrogen activation, which is a crucial step for the autocatalytic reduction mechanism observed, e.g., with bulk CuO, is not initiated unless the Cu metal nuclei formed exceed a critical size.

Experimental Section

Materials. Silicalite-1 (Si/Al > 240) and Na-ZSM-5 (Si/Al = 14) were kindly donated by Süd-Chemie AG and Chemiewerk Bad Köstritz, Germany, respectively. Dealuminated Y ("DA-Y") was a material produced by Degussa AG via the $SiCl_4$ dealumination route, which avoids the creation of mesopores. The synthesis of MCM-48 has been described elsewhere,[17] together with characterization data. In powder diffraction, the (211) reflection was found at $2\theta = 2.70°$ (d spacing, 3.272 nm) while N_2 physisorption yielded an average pore diameter of 2.5 nm, which is, however, subject to considerable uncertainty due to inaccuracies of the BJH formalism in this pore-size region.

* Corresponding author: Professor W. Grünert, Lehrstuhl für Technische Chemie, Ruhr-Universität Bochum, P.O. Box 102148, D-44780 Bochum, Germany; tel, +49 234 322 2088; fax, +49 234 321 4115; e-mail, w.gruenert@techem.ruhr-uni-bochum.de.

† Lehrstuhl für Technische Chemie, Ruhr-Universität Bochum.

‡ On leave from: N. D. Zelinsky Institute of Organic Chemistry, Russian Academy of Sciences, Moscow, Russia.

§ Hasylab, Hamburg, Germany.

|| On leave from: Department of Chemical Engineering, Istanbul University, 34850 Istanbul, Turkey.

⊥ Lehrstuhl für Kristallographie, Ruhr-Universität Bochum.

Lehrstuhl für Physikalischen Chemie I, Ruhr-Universität Bochum.

10.1021/jp054033i CCC: $30.25
Published on Web 10/18/2005

TABLE 1: Samples Used in the Present Study: Composition (by ICP) and Surface Analytical Results

sample code	matrix	wt % Cu	Cu/Si	$(Cu/Si)_{XPS}$	α_{Cu},[a] eV
Cu-Sil	silicalite-1	1.1	0.010_5	0.040	1847.1
Cu-DAY	DA-Y	1.1	0.010_5	0.007	1846.9
Cu-MCM-48(1)	MCM-48	1.2	0.011_5	0.008	1846.9
Cu-MCM-48(6)	MCM-48	5.6	0.054	0.060	1846.6
Cu-ZSM-5	ZSM-5	3.2_5	0.032	0.082	1846.6

[a] α_{Cu} is Auger parameter; α_{Cu} = BE (Cu(2p)) + KE (CuLVV) (for primary data, see ref 22; CuO, α_{Cu} = 1851.5 eV; Cu_2O, α_{Cu} = 1849.5 eV).

Copper was introduced into Na-ZSM-5 by 3-fold aqueous exchange of Na-ZSM-5 with 0.01 M Cu acetate solution. MCM-48 was loaded with Cu species by soaking it in Cu acetate solution the concentration of which was varied to obtain different Cu contents. The liquid was then decanted and replaced by a fresh solution twice before the solid was filtered off. The copper-containing ZSM-5 and MCM-48 materials were dried at room temperature and at 423 K and calcined in air at 800 or 823 K. The introduction of Cu into silicalite-1 and DA-Y took advantage of the mobility of Cu(I) species that migrate even into the Na form of zeolites at elevated temperatures.[18] The supports were soaked in a 0.01 M ethanolic copper acetate solution under reflux at 333 K for 22 h. Subsequently, the samples were dried, heated in flowing N_2 at 823 K for 4 h to induce the reduction of Cu(II) to Cu(I) and the diffusion of the latter into the pore system, and calcined in synthetic air (20% O_2 in N_2) at 673 K.

The intraporous location of the Cu species was confirmed by a combination of X-ray photoelectron spectroscopy (XPS) and X-ray-induced Auger electron spectroscopy (XAES), where a high dispersion of ionic copper species as in intrazeolite positions leads to dramatic changes of the Auger parameter.[19−21] The spectra obtained have been given in a preliminary communication,[22] and the data are summarized in Table 1 together with results for an additional sample (Cu-MCM-41(1)) and with the Cu contents, which were determined by inductively coupled plasma optical emission spectroscopy and confirmed by assessments via the Cu K XAFS step heights. The Cu content in the siliceous matrixes is ≈1 wt %, but with MCM-48, a higher loaded sample was also studied. The almost fully exchanged Cu-ZSM-5 (Cu/Al ca. 0.45) was originally selected just to confirm the two-step reduction scheme reported by many authors, but the runaway phenomenon occurring with this sample (cf. Figure 1a) proved it to be of particular relevance for the present investigation. The XPS surface concentration data (Cu/Si atomic ratios) show that the copper distribution is quite homogeneous in MCM-48 and DA-Y while significant surface enrichment of copper is observed in the medium-pore MFI, in particular Cu-Sil. Due to these enrichment effects, the copper concentrations in the near-surface region are in the same order of magnitude for Cu-Sil, Cu-ZSM-5, and Cu-MCM-48-(6).

The CuO used as a reference material was Riedel-de Haen purum grade.

Methods. XAFS spectra (Cu K edge, 8.979 keV) were measured in transmission mode at the Hasylab E4 station (Hamburg) using a Si(111) double crystal monochromator, which was detuned to 50% of maximum intensity to exclude higher harmonics in the X-ray beam. Most experiments were performed with an in situ EXAFS cell described elsewhere,[23] in which a pressed sample is exposed to the flowing gas in a back-mixed cell volume. Since these hydrodynamic conditions have some drawbacks (no forced gas flow through catalyst, delayed water removal), some experiments were repeated in a different cell in which the gas flows horizontally through a layer of catalyst particles (250−350 μm size) held by two glass wool plugs (beam traveling in gas-flow direction). This cell is integrated into a loop scheme of gas lines, which may be opened and closed by a four-way valve in order to connect it to a gas-handling system or to detach and transfer it to a glovebox. It has been therefore also used to prepare samples for the TEM study.

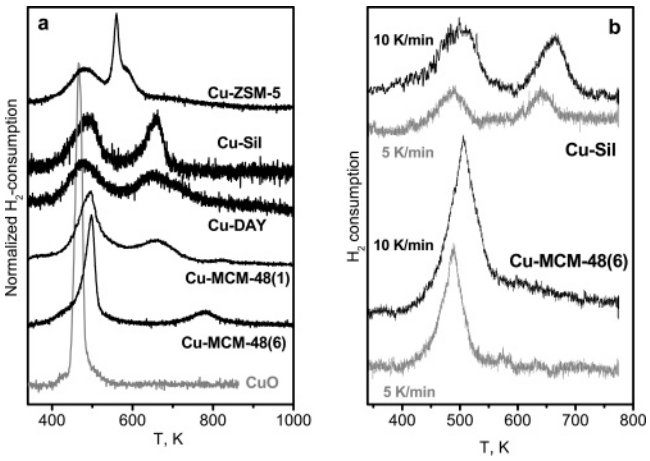

Figure 1. TPR profiles of Cu oxide species in porous matrixes, compared with CuO: (a) profiles measured at 10 K/min heating rate; (b) variation of the heating rate, study performed in a different TPR setup (see Experimental Section).

The spectra of the absorption coefficient μ were taken at liquid nitrogen temperature after the samples had been subjected to pretreatments as described below. For energy calibration, the spectrum of a Cu foil was recorded at the same time (between the second and a third ionization chamber). All spectra were measured twice to ensure reproducibility. In a typical reduction experiment, the sample was heated in flowing diluted H_2 (5% in He) to the first reduction temperature at 5 K/min and kept there for 15 min. After cooling and taking the spectrum, the previous reduction temperature was established with a 10 K/min ramp and the next temperature was approached with 5 K/min.

Data treatment was carried out using the software package VIPER.[24] A Victoreen polynomial was fitted to the preedge region for background subtraction. The smooth atomic background μ_0 was estimated using a smoothing cubic spline. The Fourier analysis of the k^2-weighted experimental function $\chi = (\mu - \mu_0)/\mu_0$ was performed with a Kaiser window. For the determination of structural parameters, theoretical references calculated by the FEFF8.10 code[25] were used. To minimize the number of free parameters, equal backscatters were fitted with the same E_o-shift wherever possible.

TPR was carried out with a mixture containing 4.2 vol % H_2 in He (84 mL/min), ramping the temperature at 10 K/min from room temperature to 1070 K. The H_2 content of the effluent was measured by a catharometry-based instrument (Hydros, Fisher-Rosemount). For technical reasons, a second series had to be carried out in a different setup that allowed maximum temperatures of 773 K only and differed slightly in the flow conditions. In this series, the influence of the heating rate on the TPR profiles was studied for two relevant samples.

Transmission electron micrographs of reduced samples were obtained with a Hitachi H-8100 microscope equipped with a LaB_6 cathode, which was operated at 200 kV. The catalysts were reduced in an in situ EXAFS flow cell (vide supra) according to the protocol used in the EXAFS study (upper end

of series only), and the reduced samples were transferred into a glovebox. There they were prepared on a TEM grid, which was inserted into a special TEM vacuum transfer holder. This holder allows transport of the reduced samples from the glovebox into the TEM in an inert argon atmosphere. It has been shown that with this vacuum transfer holder a transfer of Cu nanoparticles from the glovebox into the TEM is possible without any oxidation of the particles.[26]

Results

TPR. In Figure 1a, the TPR profiles of the copper species in porous matrixes are presented as normalized H_2 consumption (H_2/Cu) and compared with that of CuO, which is reduced in a single narrow peak around 470 K under our conditions. The overall H_2 consumption always corresponds to a complete reduction of Cu(II) to the metal, with a deviation of (−)10% for Cu-Sil, which is certainly due to higher error margins at this low Cu content (1.1 wt %). It can be seen that not only Cu-ZSM-5 but also Cu-Sil, Cu-DAY, and Cu-MCM-48(1) are reduced in a two-step pattern. The two peaks are not identical in size—in those profiles where the peaks were well separated, the consumption in the first peak was between 55% (Cu-Sil, Cu-DAY) and 67% (Cu-MCM-48(1)) of the total consumption. The profile of Cu-ZSM-5 exhibits what would be considered as an autocatalytic phenomenon: after the first maximum, which almost coincides with that in all other samples except CuO, the reduction rate increases dramatically in a narrow peak. This occurs at a 100 K higher temperature than the reduction of bulk CuO (and 70 K above the reduction of Cu in MCM-48). The reduction is, however, not complete after that, and a weak tailing extends to higher temperatures. In MCM-48, the reduction pattern of the Cu(II) species depends on the Cu content. At high Cu content (Cu-MCM-48(6)), a rapid, probably autocatalytic reduction sets on already at ≈470 K, and most of the copper is reduced below 600 K. Surprisingly, there is a second, significant hydrogen consumption at rather high temperature (around 780 K). At low Cu content (Cu-MCM-48(1)), there is a clear two-step pattern as mentioned above. Closer inspection shows also a very small high-temperature H_2 consumption analogous to that of Cu-MCM-48(6), but at an even higher temperature (820 K).

A TPR series with varied temperature ramp (Figure 1b) was performed to elucidate the origin of discrepancies between XAFS and TPR results regarding the temperatures required for complete Cu reduction in the stationary and instationary reduction regimes (vide infra). In Figure 1b, typical changes can be seen beyond the expected decrease of the signal heights with decreased heating rate. The 10 K/min profile of Cu-Sil (slightly affected by a technical problem at low temperatures) proves the good reproducibility between the two setups used: The peak temperatures agree within 10 K. The same is true for the main peak of Cu-MCM-48(6), but the high-temperature peak (cf. Figure 1a) was not seen in the repetitive run. Instead, the main (or single) reduction peak extended into a significant tailing to higher reduction temperatures. At 5 K/min, both peaks of Cu-Sil and the main peak of Cu-MCM-48(6) were slightly shifted to lower temperatures as expected. The tailing at the latter had, however, disappeared except for two weak, hardly significant features. It can be, therefore, stated that unlike the signals in Cu-Sil and the main signal in Cu-MCM-48(6) the features at the high-temperature side of the latter are not well reproducible and strongly attenuated at lower heating rates.

X-ray Absorption Spectroscopy. In Figure 2, Cu K XAFS spectra recorded after the reduction of Cu-Sil in 5% H_2/He at increasing temperatures (a, X-ray absorption near edge structure (XANES); b, Fourier transform (FT) (absolute value) of the k^2-weighted EXAFS function) are compared with the spectrum of the Cu foil. The EXAFS spectrum of the initial sample exhibits a shell at 1.45 Å (uncorrected) as well as two more weak scattering events beyond. All these signals appear at the same distances as in CuO (cf. Figure 3a), but a very strong amplitude decay suggests that the oxide clusters in the initial Cu-Sil are very small (cf. also ref 17). From the XANES, it is obvious that the reduction has already started at 405 K. With increasing temperature, the preedge peak typical of Cu(I) in Cu_2O develops in the XANES region and remains predominant up to 590 K where postedge features typical of Cu metal start to appear as well. At 650 K, the XANES is close to that of the Cu foil except for a less pronounced amplitude of the scattering features. In the EXAFS (Figure 2b), the first Cu neighbor typical of Cu metal (at 2.18 Å (uncorrected)) is clearly discernible already at 465 K, but it remains small during further temperature increment of 100 K. Only at 590 K, the first metallic Cu coordination becomes significantly stronger. At 650 K, the spectrum resembles that of the metal foil, although an asymmetry of the

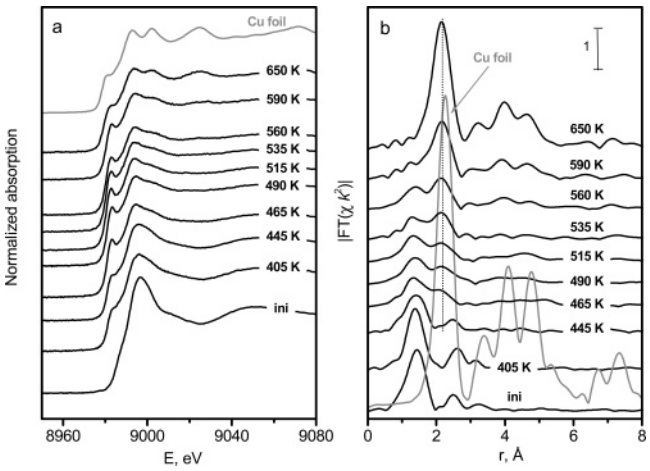

Figure 2. XAFS spectra measured after reduction of Cu-Sil at different temperatures indicated in the figure, comparison with Cu foil: a, XANES; b, EXAFS (Fourier transform (absolute value) of k^2-weighted EXAFS function). For results of model analysis, see Table 2. Spectra measured at liquid nitrogen temperature.

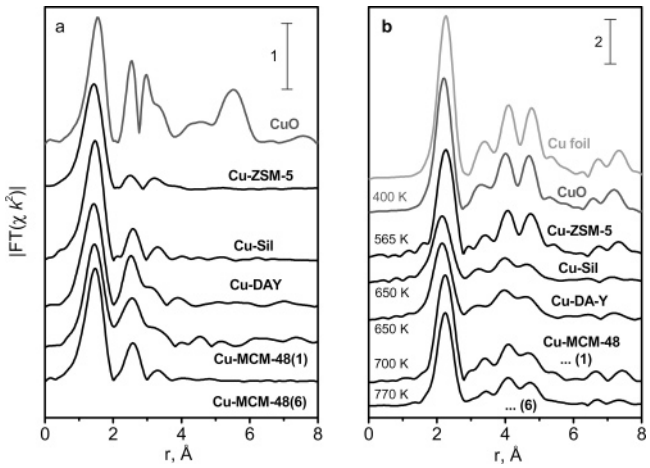

Figure 3. EXAFS spectra of copper in porous matrixes (Fourier transform (absolute value) of k^2-weighted EXAFS function): a, initial (calcined) samples; b, after reduction at temperatures indicated in the figure. Spectra measured at liquid nitrogen temperature. r_{Cu-Cu} (Å), determined by fitting of the first coordination shell: CuO, 2.54 Å; Cu-ZSM-5, 2.54 Å (565 K); Cu-Sil, 2.53 Å; Cu-DAY, 2.53 Å; Cu-MCM-48(1), 2.53 Å; Cu-MCM-48(6), 2.53 Å (650 and 770 K).

TABLE 2: Fits of EXAFS Spectra Measured after the Reduction of Cu-Sil at Different Temperatures (Figure 2)[a]

reduced at	atom	r, Å	CN	$10^3\sigma^2$, Å^{-2}	E_0, eV
initial	O[b]	1.95 ± 0.01	3.0 ± 0.3	5.0 ± 1.8	3.1 ± 1.8
405 K	O[b]	1.96 ± 0.02	1.8 ± 0.4	1.0 ± 0.1	0.3 ± 2.6
	O	1.84 ± 0.03	0.8 ± 0.3	2.9 ± 2.8	0.7 ± 4.5
425 K	O[b]	1.95 ± 0.02	1.3 ± 0.2	3.6 ± 2.7	9.2 ± 2.5
	O	1.86 ± 0.02	1.0 ± 0.2	2.6 ± 2.6	10.3 ± 2.7
445 K	O[b]	1.95 ± 0.01	1.1 ± 0.1	2.3 ± 1.7	9.6 ± 4.7
	O	1.86 ± 0.01	1.4 ± 0.1	8.4 ± 2.6	9.2 ± 0.1
	(Cu)	(2.55 ± 0.01)	(0.2± 0.1)	(2.0 ± 32)	(11.6 ± *[c])
465 K	O	1.87 ± 0.01	1.5 ± 0.1	6.9 ± 2.1	8.6 ± 1.2
	Cu	2.53 ± 0.02	1.3 ± 0.4	0.9 ± 3.3	4.7 ± 2.2
490 K	O	1.87 ± 0.02	1.4 ± 0.1	8.4 ± 2.7	7.8 ± 2.7
	Cu	2.53 ± 0.02	1.5 ± 0.5	9.4 ± 4.0	5.8 ± 2.1
515 K	O	1.86 ± 0.02	1.4 ± 0.1	7.9 ± 2.7	8.1 ± 1.4
	Cu	2.53 ± 0.02	1.6 ± 0.6	0.9 ± 4.2	4.9 ± 2.2
535 K	O	1.86 ± 0.02	1.3 ± 0.1	9.4 ± 3.2	6.2 ± 1.6
	Cu	2.52 ± 0.02	1.9 ± 0.5	9.5 ± 3.1	5.8 ± 1.9
560 K	O	1.86 ± 0.02	1.2 ± 0.1	8.4 ± 4.4	6.0 ± 2.4
	Cu	2.53 ± 0.02	2.5 ± 0.8	9.9 ± 3.8	5.6 ± 3.8
590 K	O	1.86 ± 0.03	0.9 ± 0.1	8.9 ± 3.9	5.1 ± 3.3
	Cu	2.53 ± 0.01	3.1 ± 0.4	7.2 ± 1.0	4.2 ± 1.3
650 K	O	1.86 ± 0.01	0.4 ± 0.4	9.4 ± 31	4.5 ± *[c]
	Cu	2.53 ± 0.02	6.9 ± 0.9	4.7 ± 1.3	5.3 ± 1.7

[a] Cu−O distances constrained to 1.94 Å < r_1 < 1.97 Å and to 1.84 Å < r_2 < 1.87 Å (see text). Cu foil at liquid-nitrogen temperature: $r_{(Cu-Cu)}$ = 2.543 ± 0.002 Å. CN = 11.9 ± 0.3. [b] Additional shells: initial, 1.2 Cu at 2.89 Å; 405 K, 0.9 Cu at 2.87 Å; 425 K, 0.4 Cu at 2.88 Å; 445 K, 0.2 Cu at 2.91 Å. [c] No result for error.

first scattering peak implies that some Cu ions may have survived. Some other deviations from the spectrum of the foil should be noted. There is a significantly lower intensity of the first (Cu(0)−Cu) shell and a clear amplitude decay: the features at 4.0 and 4.7 Å (uncorrected), which are of almost equal intensity in the Cu foil, differ in the reduced Cu-Sil, and the scatterers beyond 6 Å (uncorrected) are hardly significant. Also, the subshells between 3 and 6 Å (uncorrected), which are well separated in the Cu foil, are smeared out in the reduced Cu−Sil, and they peak at slightly different r values, as does the first (Cu(0)−Cu) coordination shell (see Figure 3b, legend).

The XAFS spectra obtained in analogous reduction series with most other samples discussed in this paper (except for Cu-MCM-41(1)) have been shown previously[22] where, however, numerical results have been given only for some examples. The present paper is focused on the quantitative analysis of the spectra and the conclusions thereof; hence the presentation of primary spectra is confined to those of Cu-Sil (Figure 2) and to a comparison of the spectra obtained with the initial samples (Figure 3a) and of the Cu metal phase formed at the highest reduction temperatures (Figure 3b). Figure 3a demonstrates that the structure of the initial Cu oxide phase is rather similar in the different matrixes. In all cases, there are scattering events at the same distances as in CuO, but with a strong amplitude decay, i.e., small aggregates of CuO short-range order have been formed. These aggregates are smallest in Cu-ZSM-5. Remarkably, the scattering features of the higher shells are somewhat larger in Cu-MCM-48(1) than in Cu-MCM-48(6); i.e., larger clusters have been formed at smaller Cu content.

In Table 2, the results of the model analysis of the first shell are summarized for Cu-Sil after reduction at different temperatures to exemplify the strategy of data treatment and presentation. It is obvious from Figure 2 that many of the spectra reflect the coexistence of different Cu oxidation states. Such a situation is often analyzed by treating the XANES of a mixture as a linear combination of component contributions, which can be identified by principal component analysis. This approach is, however, inappropriate in our case because the XANES of the highly disperse species present in the sample are different from those of bulk-phase materials (Cu oxides, Cu metal) which could be used as references. There are indications that the XANES of small particles vary with changing dispersion,[27] and our data contain nice illustrations for this as well. Thus, all scattering features are less pronounced in the XANES of reduced Cu-MCM-48(6)[22] than in that of the Cu foil although both contain exclusively zerovalent copper. Among the data presented in the present paper, a similar comparison can be made between the XANES of Cu-Sil reduced at 650 K and of the Cu foil (Figure 2a): the minor amounts of cuprous ions, which are still present in the latter (vide infra) do not seem to affect its XANES significantly. It is therefore unpredictable how the XANES contribution of the Cu metal clusters might develop with varying particle size as apparently encountered in our samples, which renders the XANES inapplicable for practical analysis. Indeed, in attempts to assess Cu(II), Cu(I), and Cu(0) percentages on this basis, the Cu(0) contributions at intermediate temperatures, which are clearly proven in the EXAFS (Figure 2b), could not be extracted from the XANES.

We have, therefore, derived indirect information about the species distribution from EXAFS by decomposing the first shell into three contributions indicative of Cu(II), Cu(I), and Cu(0). To limit arbitrariness, the coordination distance of the oxygen shells was constrained to preselected ranges while the distance of the Cu(0)−Cu shell in the metal clusters was fitted unconstrained. The ranges of Cu−O distances were 1.94 Å < r < 1.97 Å for Cu(II) and 1.84 Å < r < 1.87 Å for Cu(I), which corresponds to the Cu−O distances in the bulk oxides (CuO, Cu_2O) with appropriate error limits. This approach, which treats the Cu ions as being part of small oxide clusters, gave acceptable fits with almost all spectra, only at low reduction degree, a fourth shell (Cu) at 2.87−2.91 Å had to be included to represent the next shell in the cluster. It should be noted that the approach actually contradicts the circumstances in alumosilicate zeolites, and it failed indeed with Cu−Y materials where Cu(II) and Cu(I) cannot be differentiated by the Cu−O distance.[16] Remarkably, it was, however, well applicable to Cu-ZSM-5 although it is not quite clear if all Cu(I) ions formed have been really detected (vide infra).

In Table 2, the reduction of Cu(II) to Cu(I) is reflected by decreasing/increasing coordination numbers (CNs) of the respective Cu−O scattering paths. The CN of the Cu(0)−Cu coordination first seen at 465 K grows only marginally over the next 100 K where Cu metal clusters and Cu(I) species coexist. The Cu(0)−Cu distance is smaller than that found for the Cu metal foil with the FEFF scattering functions used (2.543 Å). Although this difference would be within the error limits for an individual fit (Table 2), the consistent repetition of the result over seven independent runs (and with many other samples, e.g., Cu-DAY, Cu-MCM-48, cf. legend to Figure 3b) supports its significance. Such contraction has been often reported for small metal clusters. Even after reduction at 650 K, the Cu(0)−Cu CN increases only to ≈7 and the Cu(0)−Cu distance remains below the bulk value. According to a geometrical correlation derived by Borowski,[28] a CN of ≈7 ($\pm 10\%_{rel}$) indicates an average particle diameter of 9 (±1.0) Å (spherical shape assumed), which well explains the amplitude decay observed in the EXAFS spectra. However, the actual average particle size could be slightly larger because the sample still contained some ionic copper (Table 2).

To visualize the development of the CN on a common scale, we use a "normalized CN" obtained by dividing the observed

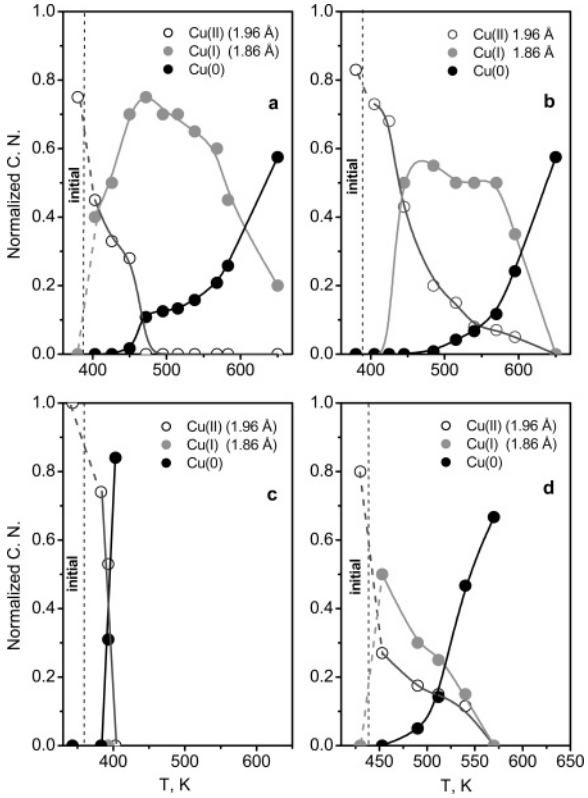

Figure 4. Reduction of CuO and of copper oxide species in MFI matrixes (stationary regime, 15 min at temperature *T*) analyzed from EXAFS spectra (fits of the first coordination shell): a, Cu-Sil; b, Cu-DA-Y; c, CuO; d, Cu-ZSM-5. Experimental coordination numbers (CN) may be obtained by multiplying the normalized CN given in the figure with 4, 2, or 12 for Cu(II), Cu(I), and Cu(0), respectively.

coordination numbers for the Cu(II)−O, Cu(I)−O, and Cu(0)−Cu paths by those in the respective bulk phases (CuO (CN = 4), Cu_2O (CN = 2), and Cu metal (CN = 12)). In Figure 4a, the results given in Table 2 are plotted in this way. It should be stressed that the normalized CN cannot directly reflect the concentration of a species in a mixture since coordination numbers of a given phase are primarily related to degrees of aggregation. However, as long as the states compared are of very high comparable dispersion, trends of the normalized CN should qualitatively reflect trends in the composition of the mixture.

In Figure 4, the reduction of Cu in microporous siliceous matrixes is compared with the reduction of Cu-ZSM-5 and of bulk CuO. Under the conditions employed, the latter proceeded in a narrow region between 385 and 405 K (Figure 4c). Only at one reduction temperature (395 K) was a coexistence of Cu oxide and Cu metal found (estimated coexistence range, 10 K). The Cu−O distance obtained from the EXAFS fit shows clearly an oxidation state of +2 for the remaining Cu oxide species, in agreement with the XANES shape. In silicalite-1, the reduction of the Cu oxide clusters passes a rather stable state between 460 and 560 K in which Cu(I) and Cu(0) coexist before further reduction of the residual copper ions (and growth of the metal aggregates) sets on (Figure 4a). Cu-DAY exhibits a similar reduction behavior, with a more narrow range of coexistence between Cu(0) and Cu ions, the latter including significant amounts of Cu(II) (Figure 4b).

The development of the normalized CN during the reduction of Cu-ZSM-5 is displayed in Figure 4d. As in the case of Cu-Sil, the formation of Cu(I) has already started at the lowest reduction temperature (here 460 K). The temperature range

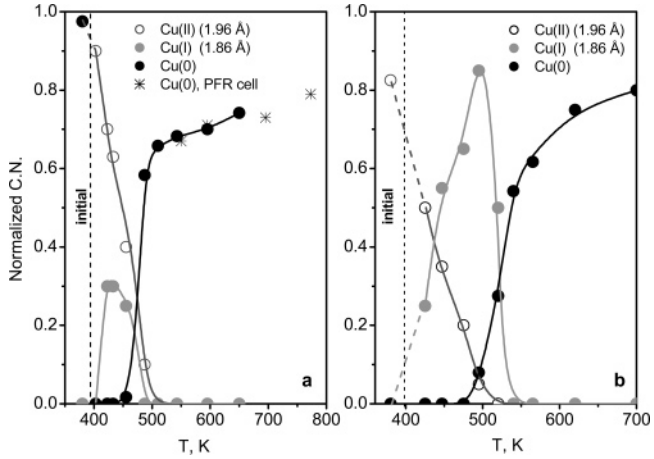

Figure 5. Reduction of copper oxide species in MCM-48 (static regime, 15 min at temperature *T*) analyzed from EXAFS spectra (fits of the first coordination shell): a, Cu-MCM-48(6); b, Cu-MCM-48-(1). Experimental coordination numbers (CN) may be obtained by multiplying the normalized CN given in the figure with 4, 2, or 12 for Cu(II), Cu(I), and Cu(0), respectively.

where Cu(0) coexists with Cu ions is smaller than that in both siliceous matrixes (≈30 K) but broader than that in CuO and at a much higher temperature than there. The Cu ions appear to be both Cu(II) and Cu(I), but it should be noted that the coordination of Cu(I) on a zeolite site may change its Cu−O distance.[16] Therefore, the Cu(II) contribution may be superimposed by a certain contribution of Cu(I) in a coordination determined by the zeolite lattice. The Cu(0)−Cu CN increases strongly at 540 K, and at 565 K it exceeds the value found with Cu-Sil after reduction at 650 K (7.6 vs 6.9). No Cu ions can be detected at this temperature, in obvious contradiction to the extended tailing of the reduction process in TPR.

The spectrum of the Cu phase at the highest reduction temperature (565 K) is given in Figure 3b. Unlike with Cu(0) in silicalite-1 or DA-Y, there is hardly any amplitude decay between 3 and 4.5 Å (uncorrected) as compared to the Cu foil, with well-defined scattering events even beyond 6 Å (uncorrected). This is in obvious contradiction to the low CN of the first Cu(0)−Cu shell (7.6) which would indicate an average diameter of 10 (±1.5) Å for spherical particles.

Figure 5 reports the development of the normalized CN during the reduction of the two Cu-MCM-48 samples. Similar to CuO, the reduction is completed in a narrow temperature interval in Cu-MCM-48(6), but this happens at much higher temperatures. Below 460 K, some Cu(I) is clearly detectable in the XANES of Cu-MCM-48(6) and also reflected by our EXAFS evaluation (Figure 5a). There is, however, only one temperature (490 K) where coexistence of metal and metal oxide species (Cu(II)) occurs. Above 500 K, the Cu(0)−Cu CN increases only moderately while Cu ions, which might be expected from the 10 K/min TPR profiles in Figure 1, cannot be detected. Figure 5a contains also data points measured with forced flow through a bed of catalyst particles (instead of a pressed pellet in a backmixed gas volume, cf. Experimental Section). The coordination numbers found are slightly smaller, but there is no significant difference between the two reduction regimes. The coordination numbers measured increase moderately with the reduction temperature, from 7.9 at 505 K to 9.5 at 770 K, corresponding to spheres of 11 (±1.5) and 18 (±4) Å diameter, respectively.

With lower Cu content, the course of the reduction is significantly changed. Now, the intermediate Cu(I) is well observed both in XANES and in EXAFS (Figure 5b) and there

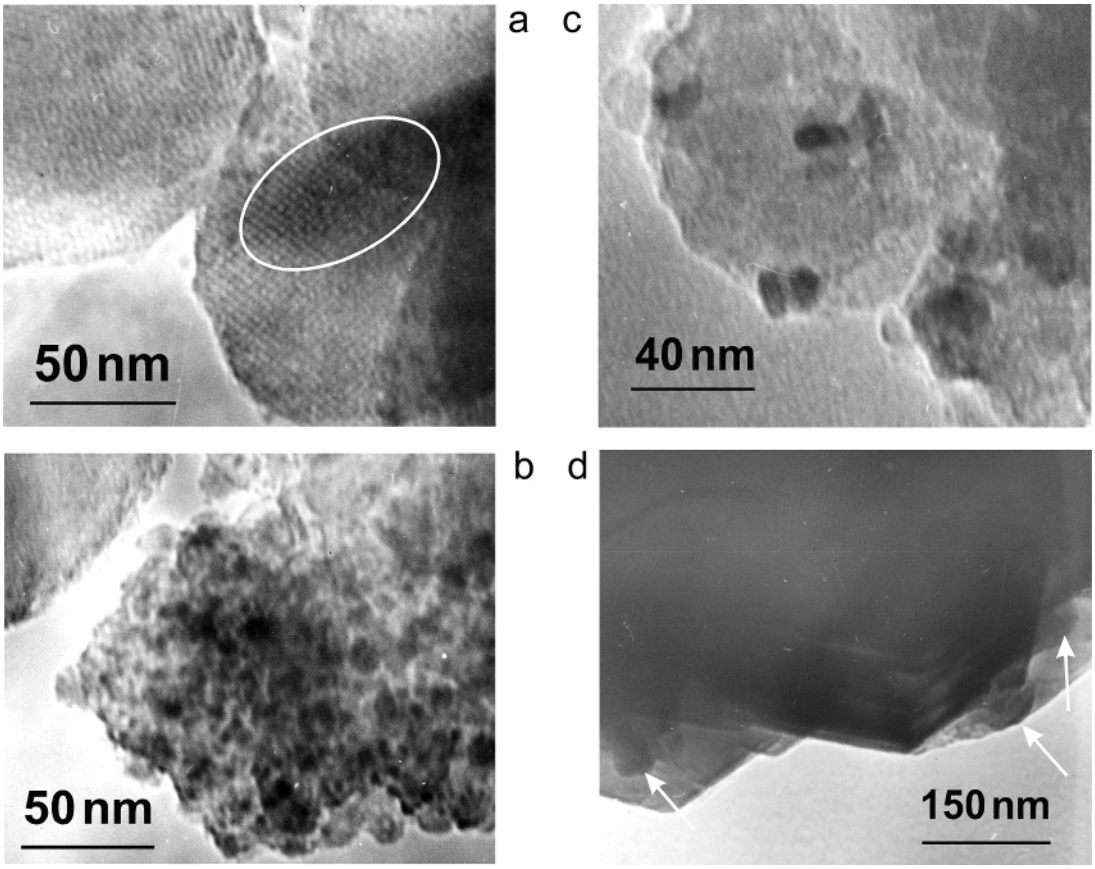

Figure 6. TEM images of reduced copper species in porous matrixes: a and b, Cu-MCM-48(6) reduced at 620 K (a, ordered matrix phase; b, amorphous minority phase); c and d, Cu-ZSM-5 reduced at 550 K.

is again clearly a temperature range in which Cu(0) and Cu(I) are found to coexist even under our stationary reduction conditions. The reduction is complete at 540 K, i.e., at somewhat higher temperature than with Cu-MCM-48(6). The Cu metal phase formed in MCM-48 resembles rather that in Cu-Sil or Cu-DAY than that in Cu-ZSM-5 (Figure 3b): The intensity of the scattering events between 3 and 4.5 Å (uncorrected) is much smaller, and the scatterers beyond 6 Å are poorly defined. Surprisingly, in Cu-MCM-48(1), the higher shells are definitely more intense than in the sample with higher Cu content, but amplitude decay is clearly present and the individual maxima of the FT are not well resolved.

Transmission Electron Microscopy. TEM micrographs have been made from Cu-Sil, Cu-ZSM-5, and Cu-MCM-48(6) reduced at temperatures where full reduction could be expected (620, 550, and 620 K, respectively), and some of them are presented in Figure 6. In reduced Cu-MCM-48(6), the periodicity of the MCM-48 pore system is well visible, and small copper particles with a size of the same order of magnitude can be seen at the intersections in several places (Figure 6a). However, a minority phase, which is obviously amorphous and exhibits a higher Cu content than the MCM material, was also found (Figure 6b). This phase contained particles of a wide size distribution, with individual clusters ranging up to 10 nm but the majority being much smaller. In Cu-ZSM-5, it was difficult to find transparent crystallites, probably owing to the origin of the sample from pressed pellets (see Experimental Section). On the external surface of the zeolite, large, bulky particles can be seen which were identified as copper by energy dispersive X-ray analysis (Figure 6c,d). No Cu particles were seen in Cu-Sil (not shown).

Discussion

As far as known materials are concerned, the data presented above agree largely with earlier studies although some remarkable differences exist. CuO is frequently used to calibrate TPR equipment for quantitative evaluation of reduction degrees, and peak temperatures around 470 K are mostly found under conditions close to ours. A similar result is reported in ref 12. In some studies, much lower reduction rates and extensive coexistence of CuO and Cu have been reported, the reduction of CuO extending over hours at 470 K.[15] On the other hand, in our XAFS study, CuO was reduced far below 470 K. We think that these deviations are due to the autocatalytic nature of the reduction[14,15] combined with the exothermicity of the overall reaction. The conditions of our standard EXAFS cell (pressed pellet, backmixed gas phase) are very unfavorable for heat removal; thus overheating effects would additionally accelerate the reduction once it has been initiated. On the other hand, very small samples flushed by a forced gas flow would minimize the temperature increase resulting in lower reduction rates observed. It has been also reported that extreme shortage of H_2 or very rapid temperature ramps change the reduction mechanism into a two-step scheme,[15] but these conditions are far from those employed in the present study.

As to Cu-ZSM-5, it should be noted that the runaway phase observed during the reduction of our Cu-ZSM-5 (Figure 1) has not been seen by most other authors[6−8,10] who report TPR profiles reminiscent of that of Cu-Sil in our study. In ref 6, an autocatalytic phenomenon during the *first* TPR peak of an overexchanged Cu-ZSM-5 was assigned to the reduction of extra-zeolite CuO. This can be safely excluded in our case not only on the basis of our surface analytical (Table 1) and EXAFS

data (Figure 3a) but also because the runaway phase starts at 100 K above the reduction of bulk CuO. We suppose that the considerable surface enrichment of the copper in Cu-ZSM-5, where the surface Cu/Si ratio of 0.08 corresponds roughly to a Cu/Al ratio of 1, is a key factor contributing to this runaway phenomenon (vide infra).

Both the TPR and the XAFS data demonstrate that the two-step reduction of Cu(II) to Cu(0) is not particular to alumosilicate zeolites. The almost identical temperature of reduction onset in Cu-Sil, Cu-DAY, and Cu-ZSM-5 (Figure 1a) suggests that the intracrystalline field of the alumosilicate MFI does not stabilize the Cu(II) ions toward reduction. Such a stabilization effect has been found in Cu-Y where a moderate upshift of reduction onset relative to Cu-DAY was observed,[16] but in ZSM-5 the field effect appears to be too weak. In Cu-ZSM-5, at least part of the Cu(I) formed showed the XAFS signature of Cu(I) in Cu_2O (unlike Cu(I) in alumosilicate FAU[16]); i.e., it seems to be not affected by a coordination geometry imposed by the zeolite lattice. Both TPR and EXAFS demonstrate that in our Cu-ZSM-5 the vast majority of the copper is reduced at even lower temperature than in Cu-Sil. Reference to the literature shows that this is due to a special effect (runaway phase) with our sample—a TPR profile similar to that of Cu-Sil would have been expected for a Cu-ZSM-5 with low exchange degree. Given the unequivocal agreement between literature sources, we have not included such a sample in our study.

The comparison between the TPR profiles and the stationary reduction runs with subsequent XAFS analysis reveals an apparent contradiction with respect to the temperatures at which the reduction is completed. It is clear that in TPR, reduction features will appear at higher temperatures than those in the stationary reduction regime due to the transformation of the reduction kinetics onto the temperature scale. The difference between the temperatures of events in TPR and in the XAFS studies is, however, very different for different events. For Cu-Sil, the temperature region of minimum reduction rate as seen by EXAFS can be identified in Figure 4a where little conversion of Cu(I) happens between 470 and 570 K, while in TPR the valley between the peaks extends between 520 and 620 K (Figure 1). This results in a shift of roughly 50 K. In Cu-ZSM-5, where the separation between the two TPR peaks is less distinctly reflected in the EXAFS spectra, the reduction goes on at a low rate up to ≈800 K in TPR (Figure 1) while according to EXAFS there is definitely no ionic Cu left at 570 K (Figure 4d). While the small Cu percentage reduced in this tailing may have escaped detection in XAFS, the contradiction is more obvious in Cu-MCM-48(1) and, in particular, in Cu-MCM-48-(6). The latter was fully reduced at 520 K in the stationary regime (see Figure 5a) while in TPR a peak centered at 780 K occurred representing ca. 20% of the total H_2 consumption (i.e., up to 40% of the copper if present as Cu(I) (Figure 1a)). The complementary TPR series with heating ramp variation (Figure 1b) shows, however, that this high-temperature feature tends to disappear at lower heating rates and is not well reproducible. The following discussion will have to offer an explanation for these observations.

An important result of our EXAFS study is the fact that the two sometimes well-separated reduction peaks in the TPR of Cu(II) in porous media cannot be identified with the conversions of all Cu(II) to Cu(I), and further of Cu(I) to Cu(0). Even in those samples where one may be tempted to ascribe the difference between the TPR peak areas to experimental errors (Cu-Sil, Cu-DAY), the EXAFS spectra show clearly that the product of the first phase is actually a mixture of Cu ions (mostly Cu(I)) and Cu(0), which is stable over a wide temperature range. In these siliceous matrixes, the Cu(0) forms apparently very small clusters. This cannot be directly concluded from the small EXAFS CN (Table 2) due to the simultaneous presence of Cu-(I) species, but the small Cu(0)−Cu distances consistently found definitely exclude a situation where the Cu(0) signal arises from a minority of large Cu particles outside the zeolite crystals. However, also in Cu-ZSM-5, there is a coexistence of small Cu(0) clusters with Cu ions over a certain temperature range. The rapid reduction phase starts delayed from an intermediate relatively stable state with Cu(0) already present. Only in Cu-MCM-48(6) does the formation of the metal proceed essentially in one step (although at higher temperature than with bulk CuO) and EXAFS sees almost no coexistence between Cu(0) and ionic states.

The reduction of bulk transition-metal oxides is thought to proceed autocatalytically, activation of hydrogen by metal nuclei formed causing the acceleration of the reduction of remaining oxide material. The mechanism can be enhanced by overheating of the sample due to insufficient heat transfer. Indeed, a runaway phenomenon does not unambiguously indicate an autocatalytic step because it could be caused also by heat transport limitations. However, in Cu-ZSM-5 the steep rise of the reaction rate starts off from a rate minimum, which clearly contradicts the assumption of a simple temperature runaway phenomenon. With Cu nuclei being formed in all porous samples in the same temperature region, the question arises as to which is the origin of the very different course of further reduction.

To answer this question it is useful to compare the Cu(0) particles found in different matrixes at the highest reduction temperatures (Figure 3b). The reduction of bulk CuO at the very low temperature of ≈400 K results in rather disperse Cu metal—the Cu(0)−Cu CN obtained (10.5) corresponds to an estimated average particle diameter of 30−40 Å. It is quite obvious from the TEM micrographs that in reduced Cu-ZSM-5 the external zeolite surface is decorated by large copper particles formed by segregation of copper out of the crystals during reduction. The EXAFS spectrum (cf. Figure 3b) supports this by its close analogy to that of the Cu foil, except for the CN of the first Cu(0)−Cu sphere which suggests an average particle diameter (≈10 Å) too small to allow for intense scattering events at 6−8 Å (uncorrected). We conclude, therefore, that along with the extra-zeolite Cu aggregates, there is a minority of very small Cu clusters (oligomers?) left in the zeolite. The aggregation of the Cu phase is nicely reflected in the EXAFS spectra where the Cu(0)−Cu distance was as low as 2.51 Å at 510 K. The intense features between 6 and 8 Å (uncorrected, see Figure 3b) appeared already at 540 K; i.e., the formation of large particles starts between 510 and 540 K under our conditions.

The reduction of Cu(II) in silicalite (and DA-Y) results in a quite different Cu phase. No extra-zeolite particles were found in TEM images of Cu-Sil (not shown). The CN of the first Cu-(0)−Cu shell even after reduction at 650 K indicates an average particle size not much larger than the size of the channel crossings in MFI (≈9 Å; for Cu-DAY, ≈10 Å). The minute scattering events beyond 6 Å (uncorrected) can be accepted as significant only by taking into account that they were present and increasing with temperature in the whole reduction series.[22] Together with the average particle size, they indicate that at the high reduction temperatures, some larger particles may have formed, however to a much smaller extent than that seen in Cu-ZSM-5. Such particle size distribution could also explain the broadness of the features between 3 and 4.5 Å (uncorrected), which is observed in many samples (Figure 3b). The effect might

arise from a high disorder in the particles or from the coexistence of particles with smaller and larger metal−metal distances. As space constraints are absent in FAU and MCM-48, we believe that the coexistence of particles of different sizes, down to extremely small ones, is the more likely explanation.

In the spectra of the reduced Cu-MCM-48(6) sample, there is better coincidence between the average particle size predicted from the first shell and the observations with the higher shells: While average particle sizes around 20 Å are expected from the Cu(0)−Cu CN, the features above 3 Å (uncorrected) are weaker than those in all other spectra, and some scattering intensity around 8 Å (uncorrected) complies with the model. The Cu particles appear to be on the whole well confined in the MCM-48 pore system even after reduction at 770 K. In the TEM images, Cu particles associated with an amorphous minority phase the size of which exceeds the mesopore dimensions have been also found (Figure 6b). The still rather small size of these particles (which possibly represent the top end of a size distribution as well) may explain why they could not be traced from the EXAFS data. In Cu-MCM-48(1), the first Cu(0)−Cu CN of 9.6 indicates an average particle size not much different from that in Cu−MCM-48(6), and there is definitely an amplitude decay across the higher shells. On the other hand, considerable intensity is seen above 8 Å (uncorrected). The difference to Cu-MCM-48(6) could be due to a different particle size distribution in MCM-48(1), with less copper in smaller particles that do not contribute to the features above 8 Å (uncorrected).

The reduction of disperse Cu(II) oxide species may be affected by transport limitations. In the reduction of bulk CuO, hydrogen activated on the surface of Cu particles already formed reduces adjacent oxide portions. It has been found that in this process hydrogen diffuses into the CuO lattice causing a lattice expansion.[15] In our XAFS study of disperse oxide phases, we have no evidence for such lattice expansion, but our EXAFS analysis via decomposition of the first scatterer into three contributions (vide supra) may have been too coarse for this purpose. In our porous matrixes, small Cu oxide clusters are initially spread over the pore systems (Figure 3a), and even where samples are strongly surface enriched, it is highly unlikely that the clusters form a continuous oxide phase. Therefore, transport steps (hydrogen spillover and/or metal atom diffusion) are relevant and may become rate-limiting.

Migration of metal species is quite obvious because extrazeolite particles are found in reduced Cu-ZSM-5, and the Cu metal particles formed in most other samples (e.g., Cu-MCM-48) are apparently larger than the initial oxide clusters. The idea that the reduction of oxide clusters is *triggered* by metal atoms diffusing through the pores in the moment of their emergence is, however, discouraged by the observation of more or less extended ranges of coexistence of Cu(0) and Cu ions, even in Cu-ZSM-5 where an autocatalytic phase is finally initiated, but at a significantly higher temperature than required for the first metal nuclei to appear.

Hence, it is apparently hydrogen spillover which controls the completion of metal formation in most samples. Oxide species distant from the metal aggregates formed are reduced by spillover hydrogen, and the tailing of the reduction process (Cu-ZSM-5, Figure 1a, Cu-MCM-48(6), Figure 1b) or the high-temperature signals in the Cu-MCM-48 samples (Figure 1a) would arise from oxide species particularly remote from the metal nuclei activating the hydrogen. As for Cu-MCM-46(6) (and to a smaller extent Cu-MCM-48(1)), we believe that this sample is structurally inhomogeneous containing Cu-MCM-48 and the amorphous minority silicate phase shown in Figure 6b. Insufficiently controlled parameters of sample preparation for TPR (mixing, compacting pressure, etc.) may have caused differences in the spatial relations between the different constituents, which might be the origin of the irreproducibility of the high-temperature TPR features in this sample (Figure 1). The rate of spillover depends only weakly on temperature. Thus, the reduction of Cu oxide entities remote from the metal sites, which can proceed isothermally once the latter have been formed, will appear at higher temperatures in TPR. On the other hand, a lower heating rate will affect these features more strongly than reduction events not controlled by transport steps. The TPR study with smaller heating rate (Figure 1b) was undertaken to observe this on the high-temperature feature in Cu-MCM-48(6) (Figure 1a). The outcome was unexpected but supports the underlying assumption twice: the time expansion of the experiment virtually eliminated any high-temperature reduction feature and led already to agreement with the XAFS study. At the other hand, the irreproducibility regarding the shape of these features in the 10 K/min runs is an additional support for transport effects in the reduction of this structurally inhomogeneous material. Therefore, reduction features extending to much higher temperatures in TPR than in the stationary reduction regime of the XAFS study (exceeding, e.g., the ≈50 K derived above) are probably influenced by hydrogen spillover. At the same time, one has to conclude that hydrogen spillover is not relevant for the reduction of Cu-Sil and Cu-DAY.

This raises the question why Cu nuclei coexisting with Cu oxide species during the reduction of most samples (except Cu-MCM-48(6)) did not trigger the immediate reduction of the remaining oxide species. Possible answers to this question are that the Cu ions coexisting with Cu(0) could not be reduced by the activated hydrogen offered or that the metal nuclei present are unable to provide activated hydrogen. The first version is highly unlikely on the grounds of our experimental data. Indeed, what could discriminate Cu oxide species in ZSM-5 to an extent that some of them are easily reduced to the metal without a source of activated hydrogen being available while others withstand reduction in *activated* hydrogen even at 20−30 K higher temperatures? Strong interactions between Cu ions and the silicate walls could be thought to explain the delay of Cu(I) reduction. However, why should the intermediate Cu(I) species be much more stable than the easily reducible Cu(II)—without an intermediate heat treatment that could result in a transformation of the material into a silicate of low reducibility. It is indeed difficult to conceive how oxide species that are swiftly reduced from Cu(II) to Cu(I) without activated hydrogen being available should be stabilized to an extent that they could withstand further reduction by activated hydrogen over the next 100 K in stationary regime. Indeed, in Cu-MCM-48(1), the reduction of which apparently involves H_2 activation and spillover, no Cu ions are left in the siliceous matrix already at a 100 K lower temperature (Figure 5b).

Thus, our data can be best explained by assuming that extremely small Cu clusters cannot activate hydrogen. Very small Cu clusters (oligomers) are obviously stabilized in porous matrixes in a certain temperature range. For Cu−Sil, the likely number of Cu atoms in them can be estimated from the space available at the channel intersections (in the order of 10 in a space of ≈7 Å diameter). Hydrogen chemisorption is an activated process over copper surfaces, and our hypothesis implies that this reaction does not proceed to an appreciable

rate on extremely small Cu particles; i.e., it is subject to a size effect. It has been found earlier in work with supported size-selected metal clusters that the catalytic reactivity of the clusters can strongly depend on their size.[29] Thus, it has been reported that the rate of CO oxidation over MgO(100)-supported Pt_n clusters decreases strongly with decreasing number of atoms n in them, decaying from a high activity at $n \geq 15$ to very low activity at $n \leq 8$,[30] while with Au_n clusters a particular high activity was observed at $n = 8$ as opposed to negligible activity at $n < 8$.[31]

The autocatalytic reduction observed in the TPR of Cu-ZSM-5 would then be a consequence of the formation of larger extra-zeolite Cu particles in this sample. The migration of Cu out of the ZSM-5 matrix may be caused by overheating or by the influence of reduction water. We believe the latter to be important as well because in Cu-Sil, the Cu clusters remain in the MFI pore system during exposure to much higher temperatures for a total of hours, Hence, the short temperature excursion during the autocatalytic phase alone would probably not suffice to induce such a dramatic displacement of matter. Once the first larger particles have been formed, the reduction of adjacent oxide species in the Cu-enriched near-surface region (now by spillover hydrogen) causes the production of more heat and water and thus the segregation of more copper from the ZSM-5 matrix, which results in the runaway phenomenon. After the runaway phase, the copper metal formed is present in large particles and is no longer well-distributed in the sample. The longer distances into the interior of the crystallites where unreduced Cu ions may have remained could be the reason for the reduction process going on for a long time (high-temperature shoulder in TPR (Figure 1a)).

In MCM-48 where the reduction starts from small oxide clusters as well, more water and heat are produced with the higher Cu content. This favors the aggregation of copper, which is however confined to the space of the pore system. Cu aggregates of 15−20 Å size can probably activate hydrogen; therefore the autocatalytic reduction mechanism is initiated at low temperature. In Cu-MCM-48(1), where less heat and water is produced, a higher temperature is required to grow particles of the critical size and initiate further reduction by spillover hydrogen. Remarkably, this happens in Cu-MCM-48(1), but not in Cu-Si and Cu-DAY, which are both silicate matrixes with almost identical Cu content. Apparently, the microporous matrixes offer more resistance to intrapore diffusion of metal atoms during the reduction process, provide more wall sites for nucleation, and confine the nuclei in a more narrow space. Therefore, the Cu clusters remain small in them even at rather high temperatures.

Conclusions

The reduction of Cu(II) oxide species in porous matrixes by hydrogen may proceed in one or in two steps. A two-step scheme as usually observed in zeolites occurs in microporous siliceous matrixes as well and cannot be explained by the stabilization of Cu ions by the intra-zeolite electrical fields. A one-step autocatalytic reduction scheme similar to that known from bulk CuO was found for CuOx clusters in mesoporous siliceous MCM-48 at high Cu content (6 wt %). In samples reduced according to the two-step scheme (Cu-ZSM-5, Cu-silicalite-1, Cu-DAY, Cu-MCM-48 of low Cu content (1 wt %)), the steps cannot be assigned to transitions from Cu(II) to Cu(I) and from Cu(I) to Cu(0). Instead, Cu(0) nuclei were formed already at low reduction temperatures and coexisted with Cu ions over temperature ranges of different extension. The temperature range of $Cu(0)/Cu^{n+}$ coexistence was narrow in materials that favor aggregation of the Cu nuclei into particles—Cu-MCM-48 of low Cu content and Cu-ZSM-5, where metal segregation from the pore system was accompanied by an autocatalytic phase in the *second* reduction step. The Cu(0) nuclei coexisted with Cu ions over a 70−100 K temperature range in the microporous siliceous matrixes that impede aggregation into large Cu particles. These observations suggest that oligomeric Cu metal nuclei which may have been formed, e.g., at the intersections of the MFI channel system, are unable to activate hydrogen which would be required for rapid reduction of the coexisting Cu ions.

Acknowledgment. The work has been funded by the German Science Foundation (DFG) in the framework of the Collaborative Research Center "Metal-substrate Interactions in Heterogeneous Catalysis" (SFB 558), which is gratefully acknowledged. Thanks are due to Mrs. Susanne Wiedemeyer and Mr. Vijay Narkhede for performing the TPR measurements.

References and Notes

(1) Busch, F.; Jäger, N. I.; Schulz-Ekloff, G.; Tkachenko, O. P.; Shpiro, E. S. *J. Chem. Soc., Faraday Trans.* **1996**, *92*, 693.

(2) Narayana, M.; Michalik, J.; Contarini, S.; Kevan, L. *J. Phys. Chem.* **1985**, *89*, 3895.

(3) Shpiro, E. S.; Baeva, G. N.; Sass, A.; Shvets, V. A.; Fasman, A. B.; Kazanskii, V. B.; Minachev, K. M. *Kinet. Katal.* **1987**, *28*, 1432.

(4) Contarini, S.; Michalik, J.; Narayana, M.; Kevan, L. *J. Phys. Chem.* **1986**, *90*, 4586.

(5) Sarkany, J.; Sachtler, W. M. H. *Zeolites* **1994**, *14*, 7.

(6) Bulanek, R.; Wichterlová, B.; Sobalik, Z.; Tichy, J. *Appl. Catal., B* **2001**, *31*, 13.

(7) Torre-Abreu, C.; Henriques, C.; Ribeiro, F. R.; Delahay, G.; Ribeiro, M. F. *Catal. Today* **1999**, *54*, 407.

(8) Torre-Abreu, C.; Ribeiro, M. E.; Henriques, C.; Delahay, G. *Appl. Catal., B* **1997**, *14*, 261.

(9) Neylon, M. K.; Marshall, C. L.; Kropf, A. J. *J. Am. Chem. Soc.* **2002**, *124*, 5457.

(10) Da Costa, P.; Modén, B.; Meitzner, G. D.; Lee, D. K.; Iglesia, E. *Phys. Chem. Chem. Phys.* **2002**, *4*, 4590.

(11) Yamaguchi, A.; Shido, T.; Inada, Y.; Kogure, T.; Asakura, K.; Nomura, M.; Iwasawa, Y. *Catal. Lett.* **2000**, *68*, 139.

(12) Günter, M. M.; Ressler, T.; Jentoft, R. E.; Bems, B. *J. Catal.* **2001**, *203*, 133.

(13) Grunwaldt, J.-D.; Caravati, M.; Hannemann, S.; Baiker, A. *Phys. Chem. Chem. Phys.* **2004**, *6*, 3037.

(14) Rodriguez, J. A.; Kim, J. Y.; Hanson, J. C.; Perez, M.; Frenkel, A. I. *Catal. Lett.* **2003**, *84*, 247.

(15) Kim, J. Y.; Rodriguez, J. A.; Hanson, J. C.; Frenkel, A. I.; Lee, P. I. *J. Am. Chem. Soc.* **2003**, *125*, 10684.

(16) Polarz, S.; Tkachenko, O. P.; Klementiev, K. V.; van den Berg, M. W. E.; Bandyopadhyay, M.; Gies, H.; Khodeir, L.; Muhler, M.; Grünert, W. *Phys. Chem. Chem. Phys.*, submitted.

(17) Tkachenko, O. P.; Klementiev, K. V.; Löffler, E.; Ritzkopf, I.; Schüth, F.; Bandyopadhyay, M.; Grabowski, S.; Gies, H.; Hagen, V.; Muhler, M.; Lu, L.; Fischer, R. A.; Grünert, W. *Phys. Chem. Chem. Phys.* **2003**, *5*, 4325.

(18) Liese, T.; Grünert, W. *J. Catal.* **1997**, *172*, 34.

(19) Sexton, B. A.; Smith, T. D.; Sanders, J. V. *J. Electron Spectrosc. Relat. Phenom.* **1985**, *35*, 27.

(20) Jirka, I.; Wichterlova, B.; Maryska, M. *Stud. Surf. Sci. Catal.* **1991**, *69*, 269.

(21) Shpiro, E. S.; Grünert, W.; Joyner, R. W.; Baeva, G. N. *Catal. Lett.* **1994**, *24*, 159.

(22) Tkachenko, O. P.; Klementiev, K. V.; Koc, N.; Yu, X.; Bandyopadhyay, M.; Grabowski, S.; Gies, H.; Grünert, W. *Stud. Surf. Sci. Catal.* **2004**, *154*, 1670.

(23) Kampers, F. W. H.; Maas, T. M. J.; van Grondelle, J.; Brinkgreve, D. C.; Koningsberger, D. C. *Rev. Sci. Instrum.* **1989**, *60*, 2635.

(24) Klementiev, K. V. *VIPER for Windows (Visual Processing in EXAFS Researches)*, freeware, www.desy.de/~klmn/viper.html.

(25) Ankudinov, A. L.; Ravel, B.; Rehr, J. J.; Conradson, S. D. *Phys. Rev. B* **1998**, *58*, 7565.
(26) Hambrock, J.; Becker, R.; Birkner, A.; Weiss, J.; Fischer, R. A. *Chem. Commun.* **2002**, 68.
(27) Bazin, D. C.; Sayers, D. A.; Rehr, J. J. *J. Phys. Chem. B* **1997**, *101*, 1140.
(28) Borovski, M. *J. Phys., IV* **1997**, *7*, C2−259.
(29) Heiz, U.; Sanchez, A.; Abbet, S.; Schneider, W. D. *Chem. Phys.* **2000**, *262*, 189.
(30) Heiz, U.; Sanchez, A.; Abbet, S.; Schneider, W. D. *J. Am. Chem. Soc.* **1999**, *121*, 3214.
(31) Hakkinen, H.; Abbet, W.; Sanchez, A.; U., H.; Landman, U. *Angew. Chem., Int. Ed.* **2003**, *42*, 1297.